

Kinetic self-organization of trenched templates for the fabrication of versatile ferromagnetic nanowires

B. Borca,¹ O. Fruchart,^{1,*} Ph. David,¹ A. Rousseau,¹ and C. Meyer¹

¹*Institut Néel, Department of Nanosciences (CNRS-UJF-INPG), BP166, F-38042 Grenoble Cedex 9, France*

(Dated: October 24, 2018)

We have self-organized versatile magnetic nanowires, *i.e.* with variable period and adjustable magnetic anisotropy energy (MAE). First, using the kinetic roughening of W(110) uniaxial templates of trenches were grown on commercial Sapphire wafers. Unlike most templates used for self-organization, those have a variable period, 4-12 nm are demonstrated here. Fe deposition then results in the formation of wires in the trenches. The magnitude of MAE could be engineered up or down by changing the capping- or underlayer, in turn affecting the mean superparamagnetic temperature, raised to 175 K so far.

The bottom-up approach is promising for the fabrication of nanostructures at moderate cost, with better resolution and less microscopic defects than with lithography. In epitaxial self-organization (SO) the building blocks are atoms that aggregate to each other during growth, a process that can be engineered to fabricate wires and dots with lateral dimensions from the micron size¹ down to the atomic size^{2,3,4}. The interest of SO for fundamental research is often the narrow size dispersion⁵, so that macroscopic measurements reveal the properties of one single nanostructure. Issues like the increase of orbital momentum and magnetic anisotropy energy (MAE) at atomic edges or kinks have been addressed^{2,3,5}. Concerning applications it is sometimes argued that SO arrays could be used by addressing single nanostructures one by one, to store one bit of information for example. A more realistic view is the use of the array as a material with specific properties arising from the nanoscale. This is the case of semiconductor quantum dots with lasing properties⁶.

Do magnetic SO systems meet the requirements of applied materials? A prerequisite is that some versatility of geometrical as well as physical properties is achieved, like tuning the magnitude of the MAE. We focus here on the fabrication and properties of wires, which lie at the background of the fast-developing field of spin electronics making use of the propagation of domain walls in wires for storage or logics devices^{7,8,9}.

SO magnetic wires are often achieved by step-decoration of vicinal surfaces^{10,11,12}. This approach is not versatile as a new crystal has to be prepared with a specific miscut whenever the period needs to be changed. Templates resulting from kinetic effects are potentially more versatile as the period can be changed with processing parameters, like temperature. This has been explored using ion etching under grazing incidence to create ripples on surfaces, independently of crystalline directions¹⁴. However a significant control of the period has not been demonstrated so far. Here we explore a new approach,

based on the growth of body-centered-cubic (110) materials on nominally-flat Saphir yielding parallel trenches with an adjustable period, which we then use to grow magnetic nanowires. We could tune the magnitude of the MAE of the wires using suitably-chosen capping layers or underlayers. The use of commercial wafers while achieving some control on both the period and the MAE represents a significant advancement in the versatility of SO nanowires.

The samples were grown in a set of ultra-high vacuum chambers using pulsed-laser deposition with a Nd-YAG laser ($\lambda = 532$ nm). The chambers are equipped with a quartz microbalance, sample heating and a translating mask for the fabrication of wedge-shaped samples. A 10 keV Reflection High Energy Electron Diffraction (RHEED) setup with a CCD camera synchronized with laser shots permits operation during deposition. An Omicron room-temperature Scanning Tunneling Microscope (STM-1) and an Auger Electron Spectrometer (AES) are available. The metallic films are grown on sapphire nominally-flat (11 $\bar{2}$ 0) commercial wafers. A detailed description of the chambers and growth procedures can be found in¹⁵. The magnetic measurements were performed ex-situ on 5 nm-Mo-capped samples, with a Quantum Design Superconducting QUantum Interference Device (SQUID) magnetometer.

Ordered arrays of wires were obtained in three steps, consisting of the fabrication of 1. a non-magnetic flat buffer layer; 2. a non-magnetic template displaying a uniaxial array of trenches; 3. Fe wires by layer-by-layer deposition at the bottom of the trenches.

The first step is the preparation of a smooth buffer layer. A seed layer of Mo (nominal thickness $\Theta = 1$ nm) followed by W ($\Theta \approx 10$ nm) are deposited on sapphire at room temperature (RT) followed by annealing at 800°C. This yields a (110) surface of quality similar to that of metal single crystals, with atomically-flat terraces of width up to hundreds of nanometers^{15,16}.

The second step consists of the preparation of a non-magnetic template. It was inspired by reports of the kinetic uniaxial roughening of films of the bcc elements Fe(110)¹⁷ and W(110)¹⁸ during homoepitaxy at moderate temperature, explained by anisotropic diffusion along

*Olivier.Fruchart@grenoble.cnrs.fr

the steps and the occurrence of an Ehrlich-Schwoebel barrier. FIG. 1a (resp. c) shows the topography of a W(110) layer obtained upon deposition at 150 °C (resp. following nucleation at 550 °C and subsequent growth at 150 °C). A uniaxial array of trenches aligned along [001] is thus obtained, with a period of 4 nm (resp. 12 nm). The STM cross-sections shown as insets reveal a depth of 0.6 – 0.8 nm (resp. 2-3 nm). The structure of the trenches can be probed using RHEED with the electron beam along [001] (FIG. 1b,d). The diffraction patterns consist of arrows whose half-angle reveals the slope of the microfacets. The arrows are much sharper for trenches of larger depth because the coherence length along the facets is increased. This allows us to determine accurately the angle of the facets to $\theta = 18 \pm 1^\circ$, in perfect agreement with the triangular-like STM cross-sections of FIG. 2c. This angle is unambiguously ascribed to facets of type {210}, with $\theta = 18.43^\circ$ expected. The monitoring of RHEED patterns during growth shows that 18 ° is a stationary value, reached after a few nanometers of nominal thickness. The occurrence of a stationary angle guarantees that the shape of the trenches is not influenced by fluctuations of the width of the trenches, and thus displays essentially no distribution. This is crucial as the dispersion of MAE increases tremendously for nanosized systems in relation with the distribution of structural environments¹⁹. The existence of a stationary angle was postulated in Ref.¹⁸, however the analysis concluded to facets of type 310 with $\theta \sim 26.57^\circ$ for W. The discrepancy may come from the fact that the LEED patterns used in Ref.¹⁸ were broad because trenches with a small period were studied. We could produce templates with the same facets for Mo, Nb, V and Ta by deposition at room temperature.

The third step consists of the fabrication of wires. Fe is deposited on the templates at 150 °C (FIG. 2), for which layer-by-layer growth occurs with PLD on a smooth surface^{12,15}. For all deposits we have used W templates, which remain perfectly stable up to 300 °C. For templates of small period the surface gradually smoothes and becomes essentially flat for $\Theta = 2$ AL (Atomic Layers; not shown here). The details of the early stages of growth are easier to investigate for templates of large period. For these STM cross-sections (FIG. 2)b reveal a flat level at the bottom of the trenches, suggesting a progressive filling and thus yielding Fe wires with a triangular cross-section. Disconnected wires can be formed up to $\Theta = 2.5$ AL, beyond which percolation sets in for the 10 nm period.

We report below the magnetic properties of Fe wires prepared on W(110) templates with a mean period of 10 nm and an Fe nominal thickness of 2.5 AL. The mean thickness and width of the wires are 1 nm and 7 nm, respectively, as deduced from STM.

For Mo/Fe/W wires the easy axis of magnetization lies in-the-plane along the wires, *i.e.* along [001] (FIG. 3a). The MAE is deduced from loops along [110] like $E_a = \mu_0 \int_0^{M_s} H dM \approx 3 \times 10^5$ J/m³ at 10 K. E_a originates

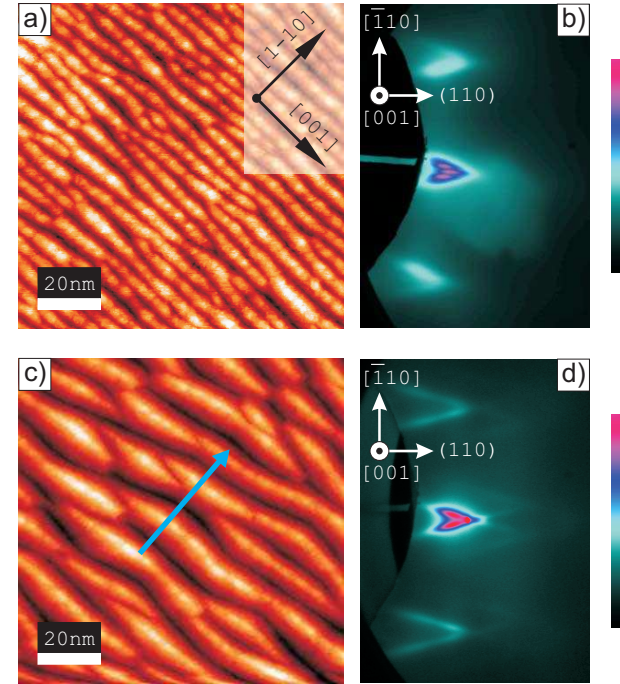


FIG. 1: W(110) templates: (a,c) 100 × 100 nm STM images of templates with small (a) and large (c) period, see text (b,d) RHEED patterns along the [001] azimuth for surfaces a and c, resp. The sample lies vertical, on the left of the patterns.

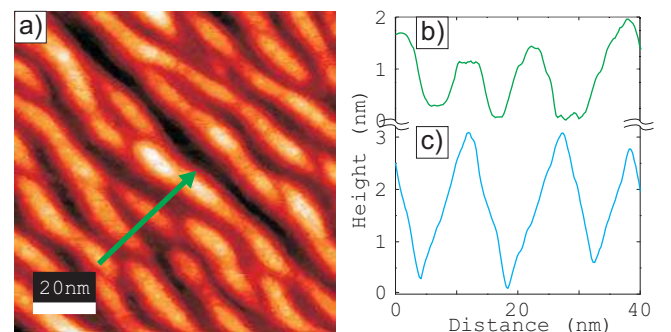


FIG. 2: (a) 100 nm STM image of wires Fe(2.5 AL)/W (b) Cross-section along the line shown in a (c) Cross-section along the line shown in FIG. 1c (same scales).

from the sum of several contributions, among which only the dipolar energy E_d can be estimated reliably. Other sources of MAE are surface (Néel-type) expected to favor the $[1\bar{1}0]$ direction for the (bottom) Fe/W interface²⁰ and $[001]$ for the (top) Mo/Fe interface²¹, step-edge for Fe/W, expected to favor $[1\bar{1}0]$ ¹⁰; magneto-elastic – unlike the case of thin films, here the large density of steps is expected to induce a significant out-of-plane mismatch and shear stress, so that no figure or even sign can be reliably predicted; finally the bulk Fe MAE is negligible. Surprisingly $E_a \approx E_d$ for this sample despite this complex situation, similarly to (Fe,Ag) self-organized arrays of wires²².

The loops measured at different temperatures with $H//[001]$ have a rather square shape, and at remanence full saturation is observed (FIG. 3b). The coercivity continuously decreases with temperature while M_s remains essentially unchanged, suggesting a superparamagnetic behavior. The ultimate blocking temperature determined by the "zero field cooling/field cooling" (ZFC-FC) process is ≈ 160 K (FIG. 3d). The mean value of T_B is around ≈ 100 K, defined as half-way up the zero-field cooling remagnetization curve.

In the following we report on the use of surface MAE to tailor the magnitude of the MAE of the wires and move towards features that would be required for applications like recording media, like functionality at room temperature and adjustment of MAE. First, the very same wires were fabricated after inserting a 1 AL-thick underlayer of Mo on the W trenches. The magnetic easy axis is again along the wires, however its magnitude is increased, which is consistent as Fe/Mo interfaces favor alignment of magnetization along $[001]$ ²¹. This brings the mean T_B from 100 K without underlayer to 175 K with underlayer (FIG. 3e). The coercive field is increased at all temperatures, compare FIG. 3b-c. On the reverse T_B is lowered to 40 K for Al/Fe/W (FIG. 3f).

Conclusion

We have demonstrated a novel route for the self-organization of arrays of planar nanowires on nominally-flat commercial wafers. It is based on the fabrication of a template of trenches upon the deposition under kinetic limitations of a non-magnetic material along a surface of uniaxial symmetry, here W(110), followed by the filling of

the bottom of the trenches by a magnetic material under layer-by-layer deposition conditions, here Fe. Periods in the range 4 – 12 nm were demonstrated. Owing to a self-limiting effect the micro-facets are all of type 210 with an angle of $\approx 18 \pm 1$ °, which is promising for attaining a low distribution of physical properties. Concerning magnetism the easy axis of magnetization lies in-the-plane along the wires. We have demonstrated the possibility to tailor its magnitude using interface MAE with different capping- or underlayers, bringing the mean blocking temperature to 175 K inserting an ultrathin underlayer

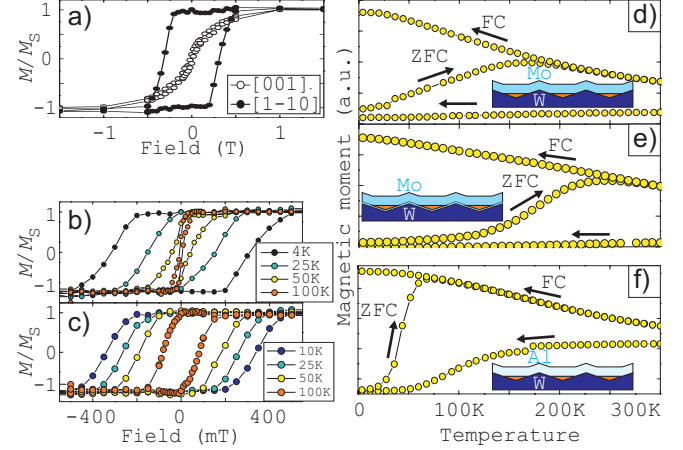


FIG. 3: Magnetization curves of Fe(2.5 AL) wires with 10 nm period. Mo/Fe/W wires (a) at 10 K in-plane along $[001]$ and $[1\bar{1}0]$ (b) in-plane along $[001]$ at different temperatures; (c) same as b, however for Mo/Fe/Mo/W wires, see text; (d-f) In-plane field-cooled (FC) and zero-field-cooled (ZFC) magnetization of (d) Mo/Fe/W (e) Mo/Fe/Mo/W and (f) Al/Fe/W wires. A schematic illustration of the samples is shown in insets.

of Mo.

B. B. and A. R. acknowledge financial support from French Région Rhône-Alpes (mobility program), and FP6 EU-NSF program (STRP 016447 MagDot), respectively.

References

- ¹ P. O. Jubert, J. C. Toussaint, O. Fruchart, C. Meyer, and Y. Samson, *Europhys. Lett.* **63**, 135 (2003).
- ² P. Gambardella, *J. Phys.: Cond. Matter* **15**, S2533 (2003).
- ³ P. Gambardella, S. Rusponi, M. Veronese, S. S. Dhesi, C. Grazioli, A. Dallmeyer, I. Cabria, R. Zeller, P. H. Dederichs, K. Kern, C. Carbone, and H. Brune, *Science* **300**, 1130 (2003).
- ⁴ J. Repp, F. Moresco, G. Meyer, K.-H. Rieder, P. Hyldgaard, and M. Persson, *Phys. Rev. Lett.* **85**, 2981 (2000).
- ⁵ N. Weiss, T. Cren, M. Epple, S. Rusponi, G. Baudot, S. Rohart, A. Tejeda, V. Repain, S. Rousset, P. Ohresser, F. Scheurer, P. Bencok, and H. Brune, *Phys. Rev. Lett.* **95**, 157204 (2005).
- ⁶ *Semiconductor Quantum Dots, NanoScience and Technology*, edited by Y. Masumoto and T. Takagahara (Springer,

Berlin, 2002).

⁷ V. Cros, O. Boulle, J. Grollier, A. Hamzí c, M. Muñoz, L. G. Pereira, and F. Petroff, *C. R. Physique* **6**, 956 (2005).

⁸ D. A. Allwood, G. Xiong, C. C. Faulkner, D. Atkinson, D. Petit, and R. P. Cowburn, *Science* **309**, 1688 (2005).

⁹ S. S. P. Parkin, U.S. patents 6834005, 6898132, 6920062.

¹⁰ J. Hauschild, U. Gradmann, and H. J. Elmers, *Appl. Phys. Lett.* **72**, 3211 (1998).

¹¹ A. Dallmeyer, C. Carbone, W. Eberhardt, C. Pampuch, O. Rader, W. Gudat, P. Gambardella, and K. Kern, *Phys. Rev. B* **61**, R5133 (2000).

¹² O. Fruchart, M. Eleoui, J. Vogel, P.-O. Jubert, A. Locatelli, and A. Ballestrazzi, *Appl. Phys. Lett.* **84**, 1335 (2004).

¹³ K. Kern, H. Niehus, A. Schatz, P. Zeppenfeld, J. Goerge, and G. Comsa, *Phys. Rev. Lett.* **67**, 855 (1991).

¹⁴ R. Moroni, D. Sekiba, F. Bautier de Mongeot, G. Gonella, C. Boragno, L. Mattera, and U. Valbusa, *Phys. Rev. Lett.* **91**, 167207/1 (2003).

¹⁵ O. Fruchart, M. Eleoui, P.-O. Jubert, P. David, V. Santonaci, F. Cheynis, B. Borca, M. Hasegawa, and C. Meyer, *J. Phys.: Cond. Matter* **19**, (2007), in press.

¹⁶ O. Fruchart, S. Jaren, and J. Rothman, *Appl. Surf. Sci.* **135**, 218 (1998).

¹⁷ M. Albrecht, H. Fritzsche, and U. Gradmann, *B* **294**, 1 (1993).

¹⁸ U. Köhler, C. Jensen, C. Wolf, A. C. Schindler, L. Brendel, and D. Wolf, *B* **454-456**, 676 (2000).

¹⁹ S. Rohart, V. Repain, A. Tejeda, P. Ohresser, F. Scheurer, P. Bencok, J. Ferré, and S. Rousset, *Phys. Rev. B* **73**, 165412 (2006).

²⁰ U. Gradmann, J. Korecki, and G. Waller, *Appl. Phys. A* **A39**, 101 (1986).

²¹ O. Fruchart, J.-P. Nozières, and D. Givord, *J. Magn. Magn. Mater.* **207**, 158 (1999).

²² B. Borca, O. Fruchart, and C. Meyer, *J. Appl. Phys.* **99**, 08Q514 (2005).